Coordination anion effects on the geometry and magnetic interaction of binuclear Dy-2 single-molecule magnets

Jinjiang Wu, Xiao-Lei Li, Léo La Droitte, Olivier Cador, Boris Le Guennic, Jinkui Tang

Journal Name

ARTICLE

Coordination anion effects on the geometry and magnetic interaction of binuclear Dy_2 single-molecule magnets

Received 00th January 20xx,
Accepted 00th January 20xx

DOI: 10.1039/x0xx00000x

www.rsc.org/

Jinjiang Wu,[a,b] Xiao-Lei Li,[a] Léo La Droitte,[c] Olivier Cador,[c] Boris Le Guennic,[c]* and Jinkui Tang[a,b]*

Two new dimeric dysprosium(III) complexes $[Dy_2(HL)_2(SCN)_2]\cdot 2CH_3CN$ (**1**) and $[Dy_2(HL)_2(NO_3)_2]\cdot 2CH_3CN\cdot 2H_2O$ (**2**) have been assembled using the H_3L multidentate ligand (H_3L = 2,2'-((((2-hydroxy-5-methyl-1,3-phenylene)bis(methylene))bis((pyridin-2-ylmethyl)azanediyl))bis(methylene))diphenol). The use of different coordination anions for the two complexes results in distinct coordination symmetries of the metal sites. The Dy centers in complexes **1** and **2** display capped octahedron and triangular dodecahedron coordination symmetry, respectively. Consequently, the two compounds exhibit distinct dc and ac magnetic properties. Complex **1** behaves as a single molecule magnet (SMM) while no SMM behavior is observed for complex **2**. Although complexes **1** and **2** possess similar core of Dy_2O_2, their different coordination anions lead to two distinct magnetic interactions, namely ferromagnetic and antiferromagnetic for **1** and **2**, respectively. *Ab initio* calculations reveal that these interactions may result from strong intramolecular dipolar couplings that are ferromagnetic for **1** while antiferromagnetic for **2**, while exchange couplings are antiferromagnetic in both cases.

Introduction

Single-molecule magnets (SMMs), as a new type of molecular nanomagnets, exhibit magnetic bistability and slow magnetic relaxation of magnetization on a single molecule level. In recent years, SMMs have received increasingly widespread attention, which is likely due to their prospects of applications in high-density information storage, quantum computing and molecular spintronic devices.[1-7] The incorporation of lanthanide ions, especially Dy and Tb ions, leading to the booming of this field, enabled the synthesis of hundreds of high-performance SMMs, especially, mononuclear SMMs[8-10] (generally termed single-ion magnets, SIMs), which mainly benefits from the significant magnetic anisotropy of lanthanide ions.[11, 12] By virtue of intrinsic magnetic anisotropy of 4f ions, some fruitful strategies to modulate magnetic dynamics of SMMs have been applied to enhance effective energy barrier (U_{eff}) and blocking temperature (T_B), such as optimization of local symmetry and ligand environment around the spin centers[9, 13-18] or obtaining the organometallic nanomagnets in an inert atmosphere.[19-24] Until now, the mononuclear dysprosium metallocene complex $[(\eta^5\text{-Cp*})Dy(\eta^5\text{-Cp}^{iPr5})][B(C_6F_5)_4]$ (Cp^{iPr5} = pentaiso-propylcyclopentadienyl; Cp* = pentamethylcyclopentadienyl) holds the record of the highest magnetic blocking temperature of 80 K.[25] However, the quantum tunneling of magnetization (QTM) of mononuclear Ln-SMMs induces the sudden decrease of magnetization near zero field and shortens the relaxation times dramatically. Nonetheless, in polynuclear Ln-SMMs intramolecular magnetic interactions have a critical impact on the relaxation of magnetization, some of them effectively suppress the QTM in zero field.[26-32] Remarkably, benefiting from the strong couplings, dinuclear lanthanide complexes[33-35] with N_2^{3-} radical bridges exhibit a giant coercivity and the corresponding Tb_2 complex has a large blocking temperature near 30 K. In addition, some Dy_2 complexes[36, 37] featuring relatively large exchange interactions between spin centers show almost complete blockage of magnetization, indicating the relaxation pathways of quantum tunneling of magnetization are strongly suppressed. Therefore, the construction of such polymetallic complexes with large intramolecular exchange interactions represents a promising way to achieve high performance SMMs, and also provides an approach to elucidate the effect of the nature and strength of interactions between lanthanide ions on SMM behavior.

Herein, we have successfully synthesized two compounds $[Dy_2(HL)_2(SCN)_2]\cdot 2CH_3CN$ (**1**) and $[Dy_2(HL)_2(NO_3)_2]\cdot 2CH_3CN\cdot 2H_2O$ (**2**) using the multidentate ligand 3,3'-((((2-hydroxy-5-methyl-1,3-phenylene)bis(methylene))bis((pyridin-2-ylmethyl)azanediyl))bis(methylene))diphenol. In light

[a] State Key Laboratory of Rare Earth Resource Utilization, Changchun Institute of Applied Chemistry, Chinese Academy of Sciences, Changchun, 130022, P. R. China. E-mail: tang@ciac.ac.cn.
[b] School of Applied Chemistry and Engineering, University of Science and Technology of China, Hefei 230026, P. R. China.
[c] Univ Rennes, CNRS, ISCR (Institut des Sciences Chimiques de Rennes) - UMR 6226, F-35000 Rennes, France. E-mail: boris.leguennic@univ-rennesl.fr

†Electronic supplementary information (ESI) available: figures, crystallographic data, magnetic characterization. CCDC 2088272 (**1**), 2088273 (**2**). For ESI and crystallographic data in CIF or other electronic format see DOI: 10.1039/x0xx00000x

of different coordination symmetries resulting from the different coordination anions, complexes **1** and **2** display distinct magnetic relaxation behaviors. Complex **1** shows a typical SMM behavior with an effective energy barrier U_{eff} of 65.8 K and $\tau_0 = 2.22\times10^{-6}$ s, while **2** only exhibits slow magnetic relaxation. Notably, temperature dependence of the $\chi_M T$ product for the two compounds exhibit different thermal evolutions indicative of the different magnetic interactions between metal centers. The fine alteration of local symmetry on metal sites and/or the magnetic interactions between them modulate magnetic dynamics significantly. Thus, this work gives an opportunity to learn how the difference of coordination symmetries and magnetic interactions can influence the magnetic properties of SMMs.

Experimental section

General Information

All chemicals were used as commercially obtained without further purification, and all manipulations were performed under aerobic conditions. Element analysis (C, N and H) were carried out on a Perkin-Elmer 2400 analyzer. FT-IR spectra was recorded on a Nicolet 6700 Flex FTIR spectrometer equipped with a smart iTR attenuated total reflectance (ATR) sampling accessory.

Synthesis of Ligand

The ligand H_3L was synthesized according to the literature procedure.[38, 39]

Synthesis of $[Dy_2(HL)_2(SCN)_2]\cdot2CH_3CN$ (1)

Et_3N (0.15 mmol, 14 μL) was added to a solution of H_3L (0.05 mmol, 28mg) in CH_3CN (15ml). The mixture was stirred for two hours at room temperature and then $Dy(SCN)_3\cdot6H_2O$ (0.05mmol) was added. The as-obtained mixture was sealed in a glass tube of 20ml capacity and heated in an oven at 70℃ for 1 hour and then cooled to room temperature at rate of 2.5℃ /h. The light-yellow block crystals were obtained (yield: 24mg, 30% based on Dy). Elemental analysis (%) calcd for $C_{76}H_{74}Dy_2N_{12}O_6S_2$: C, 55.64, H, 4.55, N, 10.25; found: C, 55.85, H, 4.52, N, 10.31. IR (cm^{-1}):3027(w), 2912(w), 2848(w), 2051(s), 1596(s), 1569(m), 1456(m), 1450(m), 1438(m), 1365(w), 1321(w), 1255(s), 1147(m), 1114(w), 1095(w), 1045(w), 1012(w), 993(w), 966(w), 950(w), 873(w), 815(m), 748(s), 732(s), 703(m), 663(w).

Synthesis of $[Dy_2(HL)_2(NO_3)_2]\cdot2CH_3CN\cdot2H_2O$ (2)

The heat treatment procedure was similar as that used for complex **1** except that $Dy(SCN)_3\cdot6H_2O$ was replaced with $Dy(NO_3)_3\cdot6H_2O$. After cooling to room temperature, the solution was filtered. The block crystals were obtained after the slow evaporation of solvent. (yield: 30mg, 36% based on Dy). Elemental analysis (%) calcd for $C_{74}H_{74}Dy_2N_{12}O_{14}$: C, 52.89, H, 4.44, N, 10.00; found C, 52.71, H, 4.40, N, 9.97. IR (cm^{-1}): 3062(w), 2825(w), 2360(w), 2339(w), 1594(m), 1569(w), 1481(s), 1456(s), 1295(m), 1263(s), 1178(m), 1147(m), 1099(w), 1031(m), 1012(w), 991(w), 944(w), 931(w), 892(w), 873(w), 815(m), 794(m), 754(s), 740(s), 659(w), 649(w).

Crystallography

The structures of **1** and **2** were determined at 173 K on a Bruker AXS D8 Venture single-crystal diffractometer equipped with graphite-monochromatized Cu Kα radiation (λ = 1.542 Å) and graphite-monochromatized Mo Kα radiation (λ = 0.71073 Å). The structures were determined with the ShelXT[40] structure solution program using the Intrinsic Phasing solution method and by using Olex2[41, 42] as the graphical interface. The model was refined with a version of ShelXL[40] using Least Squares minimisation. All non-hydrogen atoms were refined anisotropically. Most hydrogen atom positions were calculated geometrically and refined using the riding model, but some hydrogen atoms were refined freely.

Magnetic susceptibility measurements.

Magnetic data were carried out on a Quantum Design MPMS-XL7 SQUID magnetometer equipped with a 7 T magnet. The direct current (dc) data were collected with an external magnetic field of 1000 Oe in the temperature range of 1.9−300K, and alternating current data were recorded in a 3 Oe ac field oscillating at different frequency from 1 to 1488 Hz. The experimental magnetic susceptibility data are corrected for the diamagnetism estimated from Pascal's tables[43] and sample holder calibration.

Computational details

Atomic positions were extracted from the crystal structures obtained by X-ray diffraction. Only the positions of the hydrogen atoms have been optimized at the DFT level using the 2017 release of the Amsterdam Density Functional (ADF) package,[44-46] while other atom positions were kept frozen. The calculations employed the revPBE[47, 48] functional, the triple-ζ polarized all-electron Slater type basis (TZP) from the ADF basis-set library, used the scalar relativistic (SR) all-electron zeroth-order regular approximation (ZORA) Hamiltonian[49] and were performed in the unrestricted formalism by considering an open-shell doublet spin state.

Wavefunction-based calculations were performed using the State-Averaged Complete Active Space Self-Consistent Field approach with Restricted-Active-Space-State-Interaction method (SA-CASSCF/RASSI-SO), as implemented in the *OpenMolcas* quantum-chemistry package.[50] In this approach, the relativistic effects are treated in two steps on the basis of the Douglas–Kroll Hamiltonian.[51] The scalar terms are included in the basis-set generation and are used to determine the CASSCF wavefunctions and energies.[52] Spin-orbit coupling is then added within the RASSI-SO method, which mixes the calculated CASSCF wavefunctions.[53, 54] Spin−orbit (SO) integrals are calculated using the AMFI (atomic mean-field integrals) approximation.[55] The resulting spin-orbit wavefunctions and energies are used to compute the magnetic properties and g-tensors of the ground state and excited states multiplets following the pseudospin $\boldsymbol{S}$ = 1/2 formalism, as implemented in the SINGLE_ANISO routine.[56] Cholesky decomposition of the

bielectronic integrals was employed to save disk space and to speed up the calculations.[57]

Complexes **1** and **2** are centrosymmetric binuclear compounds. Thus, calculations were only performed on one Dy^{III} center while the second Dy^{III} center was replaced by the closed-shell Y^{III} ion. The active space considered in the calculations consisted of the nine 4f electrons of the Dy^{III} ions spanning the seven 4f orbitals, i.e. CAS(9,7)SCF. State-averaged CASSCF calculations were performed for all of the sextets (21 roots), all of the quartets (224 roots) and 224 out the 490 doublets of the Dy^{III} ion. 21 sextets, 224 quartets and 224 doublets were mixed through spin–orbit coupling in the RASSI-SO procedure. The Dysprosium and Yttrium atoms as well as the oxygen and nitrogen atoms of the first coordination sphere were described with ANO-RCC-VTZP basis sets while all the other atoms were described with ANO-RCC-VDZ basis sets.[58, 59] Dipole-dipole magnetic couplings between the two centers were then obtained using the POLY_ANISO routine.[57, 60] To better describe the interactions between the magnetic centers, we considered the exchange interaction within the Lines model,[61] which allowed us to fit the exchange values.

Results and discussion

Structure

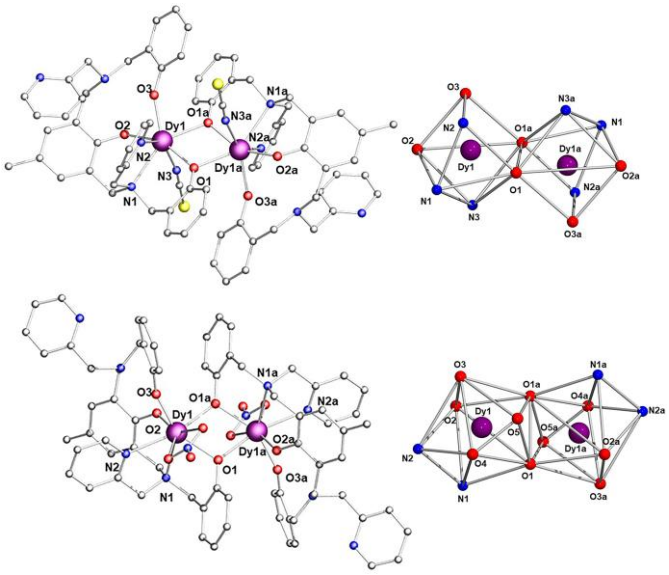

Fig. 1 Structures of compounds **1** (top) and **2** (bottom), and the coordination geometry for the Dy^{III} centers in **1** and **2**. Color code: violet, Dy; red, O; blue, N; gray, C; yellow, S; Hydrogen atoms and solvent molecules have been omitted for clarity.

Single-crystal X-ray diffraction measurements reveal that complexes **1** and **2** crystalize in the $P\bar{1}$ space group with $Z = 1$ and in the $P2_1/n$ space group with $Z = 2$, respectively. Crystal data and structure refinement details for **1** and **2** are summarized in Table S1 and selected bond distances and angles are listed in Table S2. In complex **1**, two Dy^{III} ions are bridged by the μ–O_{phenol} (O1 and O1a) resulting in the formation of Dy_2O_2 unit with Dy–O bond lengths of 2.286(3) and 2.345(1) Å, Dy···Dy distance of 3.7441(6) Å, and Dy–O–Dy angle of 107.8(7) (Fig. 1a). In addition, Dy1 ion is chelated by two N atoms (N1 and N2) from the ligand, giving the Dy–N lengths 2.623(0) and 2.529(7) Å, respectively, as well as coordinated by another two phenolic O atoms (O2 and O3) with the Dy–O lengths of 2.187(7) and 2.214(0) Å, respectively. The coordination anion SCN^- further binds each Dy center leading to a seven-coordinate N_3O_4 coordination environment with a capped octahedron (local C_{3v}) geometry (Fig. 1) as determined by SHAPE 2.0 software (Table S3).[62] Complex **2** displays a similar μ–O_{phenol} (O1 and O1a) bridged Dy_2 metal core, but with different Dy–O/N distances in the range of 2.212(5)–2.730(7) Å, Dy···Dy distance of 3.7522(5) Å and Dy–O–Dy angle of 109.6(4)°. Compared to complex **1** with coordinated anion SCN^-, NO_3^- coordinates to Dy ions in complex **2**, making another two oxygen atoms bind to metal cores. The eight-coordinate central atom displays a more distorted triangular dodecahedron coordination geometry (Fig. 1) with local symmetry of D_{2d} (Table S3).[62] Owing to the high sensitivity of axial crystal field, any slight modification of the lanthanide ion environment coordination may generate transverse components of the crystal field which results in augmentation of the QTM relaxation rate.[63-67] On account of different coordinated anions, the two compounds show totally different geometries around the Dy^{III} ions which probably results in their distinct magnetic behaviors (see below). Checking of the stacking diagrams of **1** and **2** demonstrates that the closest intermolecular Dy···Dy distances are 10.364 and 10.473 Å for **1** and **2**, respectively, indicative of negligible intermolecular magnetic exchange interactions (Fig. S1 and S2).

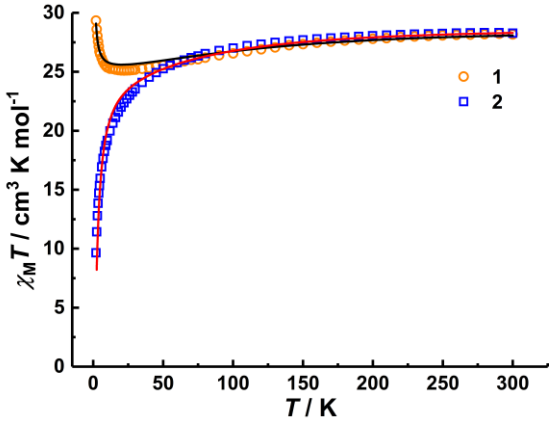

Fig. 2 Temperature dependence of the $\chi_M T$ values at 1000 Oe calculated (full lines) and measured for **1** (orange circles) and **2** (blue squares).

Direct Current (dc) Magnetism

Direct current (dc) magnetic susceptibilities data of **1** and **2** were collected on polycrystalline samples in an applied magnetic field of 1000 Oe in the temperature range of 1.9–300

K (Fig. 2). The room-temperature $\chi_M T$ values for **1** and **2** are 28.17 and 28.28 cm^3 K mol^{-1}, respectively, which are expected values for two magnetically insulated Dy^{III} ions in the $^6H_{15/2}$ ground state. The temperature dependence of magnetic susceptibilities for the two complexes displays distinct thermal evolutions. For complex **2**, $\chi_M T$ shows a slight decrease below 60 K and then a sharp decline to reach a minimum of 9.65 cm^3 K mol^{-1} at 2 K which is likely due to thermal depopulation of the Stark sublevels and/or the presence of intramolecular antiferromagnetic interactions. In contrast, $\chi_M T$ product of complex **1**, with lowering temperature, declines slightly to 25.12 cm^3 K mol^{-1} at 22 K and then rapidly increases to 29.35 cm^3 K mol^{-1} at 2 K, which accounts for the competition between the ferromagnetic interaction and the thermal depopulation of Stark sublevels of the dysprosium (III) ions. As mentioned above, intermolecular interactions could be excluded because the dimers are well isolated from each other.

Field-dependence magnetization (M) for **1** and **2** were collected in 0–70 kOe field range below 5 K. The M versus H data rise rapidly at low fields followed by a slight increase at higher fields, reaching a maximum of 10.23 μ_B for **1** and 10.00 μ_B for **2** at 7 T and 1.9 K (Fig. S3). These values are lower than the theoretical saturation value of 20 μ_B (2×10 μ_B) which mostly result from the crystal field effects for the dysprosium (III) ion.[68] Furthermore, the lack of superimposition of M *versus* H/T data (Fig. S4) on a single master curve at different temperature indicates the presence of magnetic anisotropy and/or low-lying excited state.[69] Unfortunately, there are no openings of hysteresis loops for **1** and **2** at 1.9 K (Fig. S5).

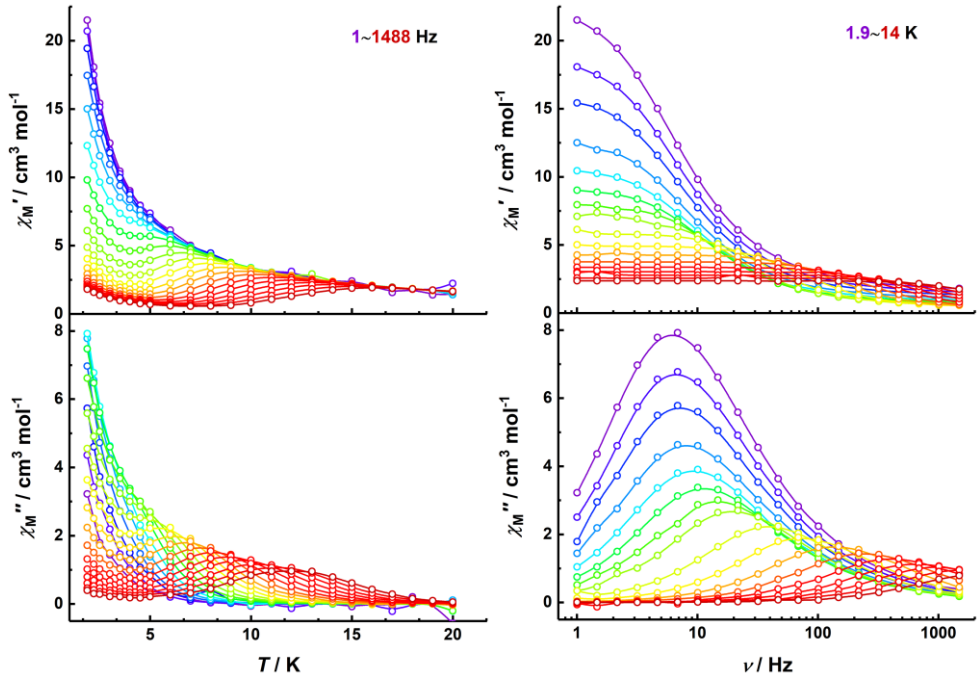

Fig. 3 Temperature (left) and frequency (right) dependence of the ac susceptibility for **1** as a function of the temperature below 20 K and the ac frequency between 1 and 1488 Hz under a zero dc field.

Alternating Current (dc) Magnetism

Alternating-current (ac) magnetic susceptibilities (Fig. 3 and Fig. S6) were measured for **1** and **2** under a zero dc field at frequencies from 1 to 1488 Hz to gain insight into dynamics of magnetization relaxation. For complex **1**, the frequency- and temperature-dependent peaks were observed in the out-of-phase χ'' *versus* T and χ'' *versus* ν plots (Fig. 3), which are characteristic of typical SMM behavior. Although the $\chi''(\nu)$ plots show a sequence of maximums in the range of 1.9–14 K, the out-of-phase peaks display temperature-independent behavior below 3.0 K, indicating the dominance of QTM relaxation process at low temperature regimes, which also can be confirmed with the appearance of increasing values of out-of-phase signals at low temperature in $\chi''(T)$ plots (Fig. 3).

From frequency-dependent ac susceptibilities curves, the relaxation time (τ) could be obtained to estimate the relaxation barrier. The plot of ln (τ) *versus* $1/T$ exhibits a linear regime at high temperature in Fig. 4, suggesting the dominance of Orbach relaxation process. QTM and Raman processes probably play the leading role at low temperatures, which is being verified by the presence of curvature and temperature-independent regimes. We have fitted the data according to eqn (1)[70]

$$\tau_{obs}^{-1} = \tau_{QTM}^{-1} + CT^n + \tau_0^{-1}\exp(-U_{eff}/T) \qquad (1)$$

where the Orbach parameters are U_{eff} and τ_0, the Raman parameters are C and n, and the rate of quantum tunneling of magnetization (QTM) is τ_{QTM}^{-1}. The best fits for complex **1** give U_{eff} = 65.8 K and $\tau_0 = 2.22\times10^{-6}$ s, C = 0.08 s^{-1}K^{-n}, n = 4.39 and $\tau_{QTM} = 2.3\times10^{-2}$ s, which is consistent with expected τ_0 of 10^{-6}-10^{-11} s for a SMM. In general, n = 7 for non-Kramers ions and n = 9 for Kramers ions, but when optical and acoustic phonons are taken into consideration, n = 1-6 is reasonable.[71] The values of C and n are within the range commonly observed for the Raman process for Dy^{III} SMMs.[24, 65, 66, 72, 73] The semicircular Cole-Cole plots (Fig. 4) from the zero field measurements can be fitted using generalized Debye model with α below 0.19

from 1.9 K to 14 K indicating a narrow distribution of relaxation times.

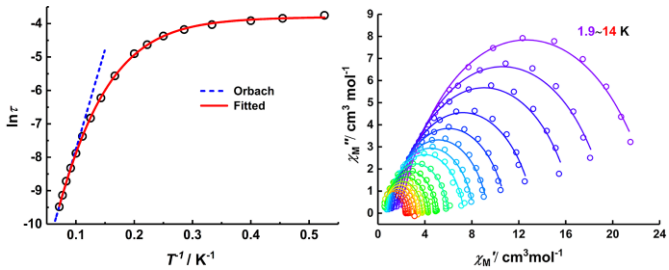

Fig. 4 Arrhenius plots (left) of relaxation time data and Cole-Cole plots (right) under zero-dc field for **1**. Solid lines correspond to the best fits.

In stark contrast to complex **1**, complex **2** displays no signals of out-of-phase ac magnetic susceptibilities in temperature range of 1.9–30 K at 997 Hz (Fig. S6). In order to investigate further magnetization relaxation behavior of **2**, the optimal dc field 1100 Oe was determined according to the field-dependent ac magnetic susceptibilities (Fig. S7). Alternating-current (ac) magnetic susceptibilities measurements (Fig. 5, Fig. S8 and Fig. S9) were carried out under 1100 Oe dc field in temperature range of 1.9–10 K from 1 to 1488Hz. The χ'' component has a strong temperature-dependence below 10 K (Fig. 5), suggesting the onset of slow magnetic relaxation. Regrettably, the expected maximums could not be observed under chosen measurement conditions. In order to evaluate U_{eff} and τ_0, another method, employed by Bartolomé et al., was performed according to the following equation, eqn (2)[74]

$$\ln(\chi''/\chi') = \ln(\omega\tau_0) + U_{eff}/T \qquad (2)$$

As shown in Fig. 5, by fitting the experimental χ''/χ' data, the parameters $U_{eff} \approx 3.4$ K and $\tau_0 \approx 1.6\times10^{-6}$ s were obtained.

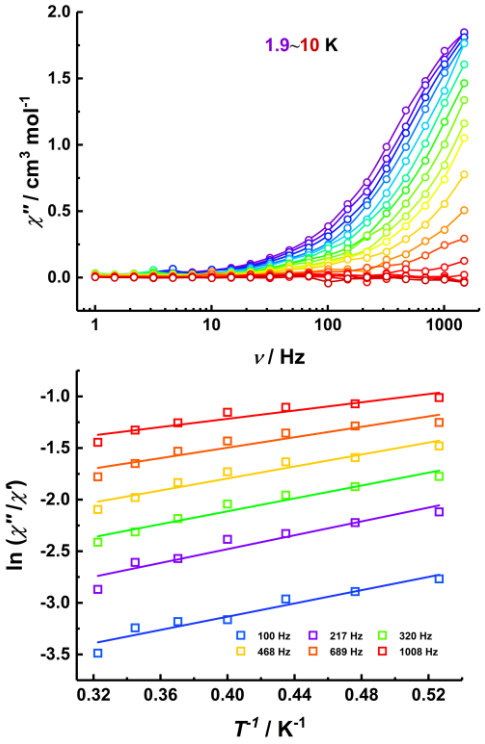

Fig. 5 Frequency dependence of the out-of-phase ac susceptibility component under a 1100 Oe applied dc field (top) and plot of ln (χ''/χ') *versus* T^{-1} (bottom) for **2**. The solid lines stand for the fits using eqn (2). (χ' and χ'' are molar in- and out-of-phase susceptibilities.)

Structural correlation

It has been well verified that the individual contribution of lanthanide centers to the magnetization blocking barrier in polynuclear SMMs[75-79] comes from a relatively weak magnetic coupling between metal centers. Therefore, the SMM performance of lanthanide complexes depends on the axiality of the ground Kramers doublet of the single ion in a weakly coupled system. Moreover, complexes **1** and **2** possess distinct geometries because of the diverse coordination anions (SCN^- for **1** and NO_3^- for **2**, respectively) coordinating to the central atom. Thus, the different magnetic relaxation behaviors for **1** and **2** may result from different coordination geometries which are likely to have an influence in nature and directions of easy axes through the crystal field.[66, 80-82] In detail, for complex **1**, the coordination geometry of each Dy^{III} ion, with a seven-coordinate coordination environment, is better to be described as C_{3v}. While the eight-coordinate Dy^{III} ion of complex **2** owns a more distorted triangular dodecahedron coordination configuration with a local symmetry of D_{2d}. In addition, intramolecular magnetic coupling interactions in polymetallic lanthanide complexes are also expected to contribute to the magnetic relaxations. It is increasingly proved that blockage of magnetization and rather long relaxation times due to magnetic interactions can be observed in several dysprosium-based SMMs.[36, 37] Note that **1** and **2** present drastic discrepancy in intramolecular magnetic coupling as shown in Fig. 2. The differences of interactions may cause the anisotropy differences of lowest exchange multiplets,

thus making a great influence in the dynamics of magnetization relaxation.[37]

Ab Initio Calculations

To investigate the magnetic properties of compounds **1** and **2**, theoretical calculations have been performed at the SA-CASSCF/RASSI-SO level on the crystal structures obtained by X-ray diffraction for each inequivalent Dy^{III} center (Computational details in Experimental Section). The overall splitting of the 2J + 1 states of **1** is about 730 cm^{-1} and its first excited state is set at 250 cm^{-1}, while the global splitting of **2** is about 559 cm^{-1} and its first excited state energy is 172 cm^{-1} (Tables S4 and S5). The ground Kramers doublets are almost pure $m_j = \pm 15/2$ for both compounds (98% for **1** and 97% for **2**), while the first excited Kramers doublet of **2** is slightly mixed $m_j = \pm 13/2$ (72%), whereas it is $m_j = \pm 13/2$ (93%) for **1**. Also, the computed magnetic transition moments (Fig. S10) tend to indicate that the slow relaxation of magnetization proceeds through the second excited state of complexes **1** and **2**, which energy is 407 cm^{-1} and 238 cm^{-1}, respectively. These values are much higher than those obtained from ac magnetic measurement for example, U_{eff} 45.7 cm^{-1} (65.8 K) in **1**. This behavior is commonly observed especially for high-nuclearity clusters[83] and one reason could be the underestimation of the Raman mechanism in the fit coupled with the role of the interaction between the magnetic centers. It is noted that the transverse transition matrix element found in this second excited state is slightly larger, inducing faster thermally assisted QTM for **2** than for **1**. These differences seem to come from the different coordination geometries between the two complexes, which can be perceived by the comparison between the Dy-O-Dy angle of 109.6° in **1** and 107.8° in **2**.

The large intermolecular Dy^{III}-Dy^{III} distances of about 10.4 Å shown in crystallographic data suggest that the intermolecular interactions are negligible. The intramolecular Dy^{III}–Dy^{III} distances are relatively short, which indicate the possibility of Dy^{III}–Dy^{III} dipolar and exchange interactions in both compounds. The intramolecular dipolar interactions are first calculated by the following equation:

$$E = \frac{\mu_0}{4\pi r^3}\left[\vec{\mu}_1 \cdot \vec{\mu}_2 - \frac{3}{\vec{r}^2}(\vec{\mu}_1 \cdot \vec{r})(\vec{\mu}_2 \cdot \vec{r})\right]$$

with *r* the Dy–Dy vector, and μ_1 and μ_2 the magnetic moment vectors of the two Dy^{III} centers. Then the exchange interaction in **1** and **2** can be fitted in relation to the experimental data by using the Lines model[61], where the following exchange Hamiltonian is employed:

$$H = -J_{dip}\tilde{S}_1\tilde{S}_2 - J_{exch}\tilde{S}_1\tilde{S}_2$$

With $\tilde{S}$ the pseudospin $\tilde{S} = 1/2$ operators at both dysprosium sites.

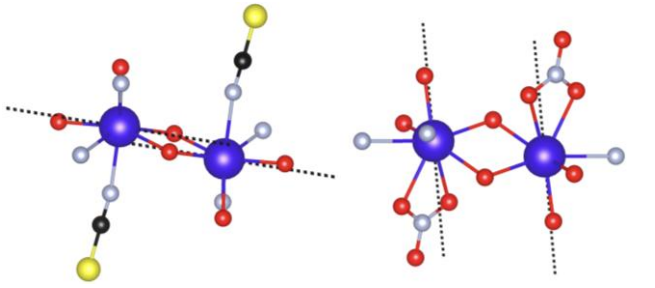

Fig. 6 Magnetic anisotropy axes representation projected on molecular structures for **1** (left) and **2** (right).

As we can see in Table 1, the exchange parameters J_{exch} are relatively close between 1 and 2 but the dipolar terms J_{dip} are very different with opposite signs. This leads to a global ferromagnetic behavior for 1 while 2 presents a strong antiferromagnetic character. Clearly, dipolar coupling drives the nature of the interaction within dimers seemingly originating from the different orientations of the magnetic anisotropy axes in both compounds.

Table 1. Best estimated exchange interaction J_{exch}, calculated dipole-dipole interaction J_{dip} and calculated total interaction $J = J_{exch} + J_{dip}$ for complexes **1** and **2**.

	J_{exch} (cm^{-1})	J_{dip} (cm^{-1})	J (cm^{-1})
1	-1.18	1.43	0.25
2	-0.76	-0.65	-1.41

The g_z values of the ground Kramers doublets of the individual Dy^{III} in **1** and **2** are 19.8 and 19.7, respectively, but the orientations of their anisotropy axes, shown in Fig. 6, give a hint on the origin of the magnetic behavior differences. Indeed, the anisotropy vectors are collinear in both compounds, but the angle between them and the Dy-Dy vector is about 15.8° for **1** and 75.8° for **2** that clearly ends with ferromagnetic dipolar coupling in **1** and antiferromagnetic in **2**. As shown in Tables S6-S7, **1** has a ferromagnetic ground exchange Kramers Doublet with a g_z value of 39.5 and a first excited exchange doublet 0.49 cm^{-1} higher, in contrary to **2** for which the ground exchange KD is not magnetic and the first excited exchange KD has an energy of 2.83 cm^{-1}. The tunneling splitting of the exchange KDs calculated for **2** and **1** are respectively about 10^{-6} and 10^{-9} cm^{-1}, resulting in a better SMM behavior for **1** than for **2**, in good agreement with experimental ac values.

These results are well illustrated in Fig. 2, where the calculated magnetic susceptibility curves well reproduce the experimental curves. The magnetic behavior of each compound appeared to be driven by the dipolar coupling existing between their two Dy^{III} centers, which is itself a consequence of their ligands coordination's geometry.

Conclusions

Two dinuclear dysprosium(III) complexes have been assembled applying the multidentate ligand (H_3L). Complexes **1** and **2** display different coordination geometries around each Dy^{III} ion because of different coordination anions. The structural difference of the two compounds not only impacts the local anisotropy on each spin center but their relative orientations,

thus leading to distinct magnetic dynamic; namely, complex **1** behaves as a single molecule magnet while complex **2** shows no SMM behavior. *Ab initio* calculations demonstrate that these properties seem to come from the strong intramolecular dipolar coupling appearing in those systems. The ligands coordination is presumably the origin of the difference of magnetic behavior between the two compounds, leading to a ferromagnetic dipolar coupling in **1** and of an antiferromagnetic dipolar coupling in **2**. Overall, it is a promising method to modulate magnetic dynamic behaviors of lanthanide complexes using different coordination anions.

Conflicts of interest

The authors declare no conflict of interest.

ORCID

Xiao-Lei Li: 0000-0002-1648-9459
Boris Le Guennic: 0000-0003-3013-0546
Jinkui Tang: 0000-0002-8600-7718

Acknowledgements

We thank the National Natural Science Foundation of China (Grants 21871247 and 21801237), Key Research Program of Frontier Sciences, CAS (Grant ZDBS-LY-SLH023), the Natural Science Foundation of Jilin Province of China (Grant 20200201244JC). J. T. gratefully acknowledges support of the Royal Society-Newton Advanced Fellowship (NA160075). L. L. D., O. C. and B. L. G. thanks the French GENCI/IDRIS-CINES centers for high-performance computing resources, and acknowledge the Stratégie d'Attactivité Durable (SAD18006 - LnCPLSMM) for financial support.

References

1. M. Atzori and R. Sessoli, *J. Am. Chem. Soc.*, 2019, **141**, 11339-11352.
2. A. Gaita-Arino, F. Luis, S. Hill and E. Coronado, *Nat. Chem.*, 2019, **11**, 301-309.
3. T. Choi, W. Paul, S. Rolf-Pissarczyk, A. J. Macdonald, F. D. Natterer, K. Yang, P. Willke, C. P. Lutz and A. J. Heinrich, *Nat. Nanotechnol.*, 2017, **12**, 420-424.
4. F. D. Natterer, K. Yang, W. Paul, P. Willke, T. Choi, T. Greber, A. J. Heinrich and C. P. Lutz, *Nature*, 2017, **543**, 226-228.
5. A. Candini, S. Klyatskaya, M. Ruben, W. Wernsdorfer and M. Affronte, *Nano. Lett.*, 2011, **11**, 2634-2639.
6. S. Sanvito, *Chem. Soc. Rev.*, 2011, **40**, 3336-3355.
7. M. Urdampilleta, S. Klyatskaya, J. P. Cleuziou, M. Ruben and W. Wernsdorfer, *Nat. Mater.*, 2011, **10**, 502-506.
8. N. Ishikawa, M. Sugita, T. Ishikawa, S. Y. Koshihara and Y. Kaizu, *J. Am. Chem. Soc.*, 2003, **125**, 8694-8695.
9. J. Wu, J. Jung, P. Zhang, H. Zhang, J. Tang and B. Le Guennic, *Chem. Sci.*, 2016, **7**, 3632-3639.
10. A. B. Canaj, S. Dey, E. R. Marti, C. Wilson, G. Rajaraman and M. Murrie, *Angew. Chem. Int. Ed.*, 2019, **58**, 14146-14151.
11. C. Benelli and D. Gatteschi, *Chem. Rev.*, 2002, **102**, 2369-2388.
12. J. D. Rinehart and J. R. Long, *Chem. Sci.*, 2011, **2**, 2078.
13. M. A. Aldamen, J. M. Clemente-Juan, E. Coronado, C. Marti-Gastaldo and A. Gaita-Arino, *J. Am. Chem. Soc.*, 2008, **130**, 8874-8875.
14. T. Morita, M. Damjanovic, K. Katoh, Y. Kitagawa, N. Yasuda, Y. Lan, W. Wernsdorfer, B. K. Breedlove, M. Enders and M. Yamashita, *J. Am. Chem. Soc.*, 2018, **140**, 2995-3007.
15. Y. S. Ding, N. F. Chilton, R. E. Winpenny and Y. Z. Zheng, *Angew. Chem. Int. Ed.*, 2016, **55**, 16071-16074.
16. K. X. Yu, J. G. C. Kragskow, Y. S. Ding, Y. Q. Zhai, D. Reta, N. F. Chilton and Y. Z. Zheng, *Chem*, 2020, **6**, 1777-1793.
17. Y. C. Chen, J. L. Liu, L. Ungur, J. Liu, Q. W. Li, L. F. Wang, Z. P. Ni, L. F. Chibotaru, X. M. Chen and M. L. Tong, *J. Am. Chem. Soc.*, 2016, **138**, 2829-2837.
18. J. Liu, Y. C. Chen, J. L. Liu, V. Vieru, L. Ungur, J. H. Jia, L. F. Chibotaru, Y. Lan, W. Wernsdorfer, S. Gao, X. M. Chen and M. L. Tong, *J. Am. Chem. Soc.*, 2016, **138**, 5441-5450.
19. F. S. Guo, B. M. Day, Y. C. Chen, M. L. Tong, A. Mansikkamaki and R. A. Layfield, *Angew. Chem. Int. Ed.*, 2017, **56**, 11445-11449.
20. C. A. P. Goodwin, F. Ortu, D. Reta, N. F. Chilton and D. P. Mills, *Nature*, 2017, **548**, 439-442.
21. P. Zhang, L. Zhang, C. Wang, S. F. Xue, S. Y. Lin and J. K. Tang, *J. Am. Chem. Soc.*, 2014, **136**, 4484-4487.
22. S. D. Jiang, B. W. Wang, H. L. Sun, Z. M. Wang and S. Gao, *J. Am. Chem. Soc.*, 2011, **133**, 4730-4733.
23. Y. S. Meng, J. Xiong, M. W. Yang, Y. S. Qiao, Z. Q. Zhong, H. L. Sun, J. B. Han, T. Liu, B. W. Wang and S. Gao, *Angew. Chem. Int. Ed.*, 2020, **59**, 13037-13043.
24. Z. Zhu, Y.-Q. Zhang, X.-L. Li, M. Guo, J. Lu, S. Liu, R. A. Layfield and J. Tang, *CCS Chem.*, 2021, **3**, 388-398.
25. F. S. Guo, B. M. Day, Y. C. Chen, M. L. Tong, A. Mansikkamaki and R. A. Layfield, *Science*, 2018, **362**, 1400-1403.
26. F. Liu, G. Velkos, D. S. Krylov, L. Spree, M. Zalibera, R. Ray, N. A. Samoylova, C. H. Chen, M. Rosenkranz, S. Schiemenz, F. Ziegs, K. Nenkov, A. Kostanyan, T. Greber, A. U. B. Wolter, M. Richter, B. Buchner, S. M. Avdoshenko and A. A. Popov, *Nat. Commun.*, 2019, **10**, 571.
27. T. Fukuda, K. Matsumura and N. Ishikawa, *J. Phys. Chem. A*, 2013, **117**, 10447-10454.
28. J. J. Le Roy, L. Ungur, I. Korobkov, L. F. Chibotaru and M. Murugesu, *J. Am. Chem. Soc.*, 2014, **136**, 8003-8010.
29. T. Pugh, N. F. Chilton and R. A. Layfield, *Angew. Chem. Int. Ed.*, 2016, **55**, 11082-11085.
30. S. Mukherjee, J. J. Lu, G. Velmurugan, S. Singh, G. Rajaraman, J. K. Tang and S. K. Ghosh, *Inorg. Chem.*, 2016, **55**, 11283-11298.
31. I. F. Diaz-Ortega, J. M. Herrera, A. Reyes Carmona, J. R. Galan-Mascaros, S. Dey, H. Nojiri, G. Rajaraman and E. Colacio, *Front. Chem.*, 2018, **6**, 537.
32. S. Ghosh, S. Mandal, M. K. Singh, C. M. Liu, G. Rajaraman and S. Mohanta, *Dalton Trans.*, 2018, **47**, 11455-11469.
33. S. Demir, M. I. Gonzalez, L. E. Darago, W. J. Evans and J. R. Long, *Nat. Commun.*, 2017, **8**, 2144.
34. J. D. Rinehart, M. Fang, W. J. Evans and J. R. Long, *Nat. Chem.*, 2011, **3**, 538-542.
35. J. D. Rinehart, M. Fang, W. J. Evans and J. R. Long, *J. Am. Chem. Soc.*, 2011, **133**, 14236-14239.

36. Y. N. Guo, G. F. Xu, W. Wernsdorfer, L. Ungur, Y. Guo, J. K. Tang, H. J. Zhang, L. F. Chibotaru and A. K. Powell, *J. Am. Chem. Soc.*, 2011, **133**, 11948-11951.
37. L. Zhang, Y. Q. Zhang, P. Zhang, L. Zhao, M. Guo and J. K. Tang, *Inorg. Chem.*, 2017, **56**, 7882-7889.
38. P. Chirakul, P. D. Hampton and Z. Bencze, *J. Org. Chem.*, 2000, **65**, 8297-8300.
39. B.-L. Lee, M. D. Kärkäs, E. V. Johnston, A. K. Inge, L.-H. Tran, Y. Xu, Ö. Hansson, X. Zou and B. Åkermark, *Eur. J. Inorg. Chem.*, 2010, **34**, 5462-5470.
40. M. Hanfland, *Acta Crystallogr. A* 2015, **71**, s3.
41. L. J. Bourhis, O. V. Dolomanov, R. J. Gildea, J. A. K. Howard and H. Puschmann, *Acta Crystallogr. Sect. A*, 2015, **71**, 59-75.
42. O. V. Dolomanov, L. J. Bourhis, R. J. Gildea, J. A. K. Howard and H. Puschmann, *J. Appl. Crystallogr.*, 2009, **42**, 339-341.
43. E. A. L. Boudreaux and L. N. Mulay, *Theory and Applications of Molecular Paramagnetism*, John Wiley & Sons, 1976.
44. G. Te Velde, F. M. Bickelhaupt, E. J. Baerends, C. Fonseca Guerra, S. J. A. Van Gisbergen, J. G. Snijders and T. Ziegler, *J. Comput. Chem.*, 2001, **22**, 931-967.
45. C. F. Guerra, J. G. Snijders, G. te Velde and E. J. Baerends, *Theor. Chem. Acc.*, 1998, **99**, 391-403.
46. E. J. Baerends, Ziegler, T., Atkins, A.J., Autschbach, J., Baseggio, O., Bashford, D., Beŕces, A., Bickelhaupt, F.M., Bo, C., Boerrigter, P.M., Cavallo, L., Daul, C., Chong, D.P., Chulhai, D.V., Deng, L., Dickson, R.M., Dieterich, J.M., Ellis, D.E., van Faassen, M., Fan, L., Fischer, T.H., Fonseca Guerra, C., Franchini, M., Ghysels, A., Giammona, A., van Gisbergen, S.J.A., Goez, A., Götz, A.W., Groeneveld, J.A., Gritsenko, O.V., Grüning, M., Gusarov, S., Harris, F.E., van den Hoek, P., Hu, Z., Jacob, C. R., Jacobsen, H., Jensen, L., Joubert, L., Kaminski, J. W., van Kessel, G., König, C., Kootstra, F., Kovalenko, A., Krykunov, M.V., van Lenthe, E., McCormack, D.A., Michalak, A., Mitoraj, M., Morton, S.M., Neugebauer, J., Nicu, V.P., Noodleman, L., Osinga, V.P., Patchkovskii, S., Pavanello, M., Peeples, C.A., Philipsen, P.H.T., Post, D., Pye, C.C., Ramanantoanina, H., Ramos, P., Ravenek, W., Rodríguez, J.I., Ros, P., Rüger, R., Schipper, P.R.T., Schlüns, D., van Schoot, H., Schreckenbach, G., Seldenthuis, J. S., Seth, M., Snijders, J.G., Sola`, M., Stener, M., Swart, M., Swerhone, D., Tognetti, V., te Velde, G., Vernooijs, P., Versluis, L., Visscher, L., Visser, O., Wang, F., Wesolowski, T.A., van Wezenbeek, E.M., Wiesenekker, G., Wolff, S. K., Woo, T.K. and Yakovlev, A.L., *Theoretical Chemistry*, 2017.
47. J. P. Perdew, K. Burke and M. Ernzerhof, *Phys. Rev. Lett.*, 1996, **77**, 3865-3868.
48. M. Ernzerhof and G. E. Scuseria, *J. Chem.Phys.*, 1999, **110**, 5029-5036.
49. E. V. Lenthe, E. J. Baerends and J. G. Snijders, *J. Chem.Phys.*, 1993, **99**, 4597-4610.
50. I. Fdez. Galván, M. Vacher, A. Alavi, C. Angeli, F. Aquilante, J. Autschbach, J. J. Bao, S. I. Bokarev, N. A. Bogdanov, R. K. Carlson, L. F. Chibotaru, J. Creutzberg, N. Dattani, M. G. Delcey, S. S. Dong, A. Dreuw, L. Freitag, L. M. Frutos, L. Gagliardi, F. Gendron, A. Giussani, L. González, G. Grell, M. Guo, C. E. Hoyer, M. Johansson, S. Keller, S. Knecht, G. Kovačević, E. Källman, G. Li Manni, M. Lundberg, Y. Ma, S. Mai, J. P. Malhado, P. Å. Malmqvist, P. Marquetand, S. A. Mewes, J. Norell, M. Olivucci, M. Oppel, Q. M. Phung, K. Pierloot, F. Plasser, M. Reiher, A. M. Sand, I. Schapiro, P. Sharma, C. J. Stein, L. K. Sørensen, D. G. Truhlar, M. Ugandi, L. Ungur, A. Valentini, S. Vancoillie, V. Veryazov, O. Weser, T. A. Wesołowski, P.-O. Widmark, S. Wouters, A. Zech, J. P. Zobel and R. Lindh, *J. Chem. Theory Comput.*, 2019, **15**, 5925-5964.
51. B. A. Hess, *Phys.Rev. A*, 1986, **33**, 3742-3748.
52. B. O. Roos, P. R. Taylor and P. E. M. Sigbahn, *Chem. Phys.*, 1980, **48**, 157-173.
53. P. Å. Malmqvist, B. O. Roos and B. Schimmelpfennig, *Chem. Phys. Lett.*, 2002, **357**, 230-240.
54. P.-Å. Malmqvist and B. O. Roos, *Chem. Phys.Lett.*, 1989, **155**, 189-194.
55. B. A. Heß, C. M. Marian, U. Wahlgren and O. Gropen, *Chem. Phys. Lett.*, 1996, **251**, 365-371.
56. L. F. Chibotaru and L. Ungur, *J.Chem. Phys.*, 2012, **137**, 064112.
57. L. Ungur, W. Van Den Heuvel and L. F. Chibotaru, *New J. Chem.*, 2009, **33**, 1224.
58. B. O. Roos, R. Lindh, P.-Å. Malmqvist, V. Veryazov and P.-O. Widmark, *J.Phys.Chem. A*, 2004, **108**, 2851-2858.
59. B. O. Roos, R. Lindh, P.-Å. Malmqvist, V. Veryazov, P.-O. Widmark and A. C. Borin, *J. Phys. Chem. A*, 2008, **112**, 11431-11435.
60. L. F. Chibotaru, L. Ungur and A. Soncini, *Angew. Chem. Int. Ed.*, 2008, **47**, 4126-4129.
61. M. E. Lines, *J. Chem. Phys.*, 1971, **55**, 2977-2984.
62. D. Casanova, M. Llunell, P. Alemany and S. Alvarez, *Chem.-Eur. J.*, 2005, **11**, 1479-1494.
63. G. Cucinotta, M. Perfetti, J. Luzon, M. Etienne, P. E. Car, A. Caneschi, G. Calvez, K. Bernot and R. Sessoli, *Angew. Chem. Int. Ed.*, 2012, **51**, 1606-1610.
64. M.-E. Boulon, G. Cucinotta, J. Luzon, C. Degl'Innocenti, M. Perfetti, K. Bernot, G. Calvez, A. Caneschi and R. Sessoli, *Angew. Chem. Int. Ed.*, 2013, **52**, 350-354.
65. C. Jin, X. L. Li, Z. Liu, A. Mansikkamaki and J. Tang, *Dalton Trans.*, 2020, **49**, 10477-10485.
66. S. Liu, J. Lu, X. L. Li, Z. Zhu and J. Tang, *Dalton Trans.*, 2020, **49**, 12372-12379.
67. I. F. Diaz-Ortega, J. M. Herrera, D. Aravena, E. Ruiz, T. Gupta, G. Rajaraman, H. Nojiri and E. Colacio, *Inorg. Chem.*, 2018, **57**, 6362-6375.
68. Y. N. Guo, X. H. Chen, S. F. Xue and J. K. Tang, *Inorg. Chem.*, 2011, **50**, 9705-9713.
69. P. H. Lin, W. B. Sun, M. F. Yu, G. M. Li, P. F. Yan and M. Murugesu, *Chem. Commun.*, 2011, **47**, 10993-10995.
70. A. F. R. Kilpatrick, F. S. Guo, B. M. Day, A. Mansikkamaki, R. A. Layfield and F. G. N. Cloke, *Chem. Commun.*, 2018, **54**, 7085-7088.
71. J. L. Liu, K. Yuan, J. D. Leng, L. Ungur, W. Wernsdorfer, F. S. Guo, L. F. Chibotaru and M. L. Tong, *Inorg. Chem.*, 2012, **51**, 8538-8544.
72. Z. Zhu, C. Zhao, T. Feng, X. Liu, X. Ying, X. L. Li, Y. Q. Zhang and J. Tang, *J. Am. Chem. Soc.*, 2021, **143**, 10077-10082.
73. J. Xiong, H. Y. Ding, Y. S. Meng, C. Gao, X. J. Zhang, Z. S. Meng, Y. Q. Zhang, W. Shi, B. W. Wang and S. Gao, *Chem Sci*, 2017, **8**, 1288-1294.
74. J. Bartolomé, G. Filoti, V. Kuncser, G. Schinteie, V. Mereacre, C. E. Anson, A. K. Powell, D. Prodius and C. Turta, *Phys. Rev. B*, 2009, **80**.
75. F. Habib, P. H. Lin, J. Long, I. Korobkov, W. Wernsdorfer and M. Murugesu, *J. Am. Chem. Soc.*, 2011, **133**, 8830-8833.

76. R. A. Layfield, J. J. McDouall, S. A. Sulway, F. Tuna, D. Collison and R. E. Winpenny, *Chem.- Eur. J.*, 2010, **16**, 4442-4446.
77. P. H. Lin, T. J. Burchell, L. Ungur, L. F. Chibotaru, W. Wernsdorfer and M. Murugesu, *Angew. Chem. Int. Ed.*, 2009, **48**, 9489-9492.
78. Y. Wang, X. L. Li, T. W. Wang, Y. Song and X. Z. You, *Inorg. Chem.*, 2010, **49**, 969-976.
79. D. N. Woodruff, R. E. Winpenny and R. A. Layfield, *Chem. Rev.*, 2013, **113**, 5110-5148.
80. M. Li, H. Wu, Z. Xia, V. Montigaud, O. Cador, B. Le Guennic, H. Ke, W. Wang, G. Xie and S. Chen, *Chem. Commun.*, 2019, **55**, 14661-14664.
81. M. Kong, X. Feng, J. Wang, Y. Q. Zhang and Y. Song, *Dalton Trans.*, 2021, **50**, 568-577.
82. F. Yang, Q. Zhou, G. Zeng, G. Li, L. Gao, Z. Shi and S. Feng, *Dalton Trans.*, 2014, **43**, 1238-1245.
83. S. Dey and G. Rajaraman, *Dalton Trans.*, 2020, **49**, 14781-14785.

SYNOPSIS TOC

The SMM behavior and the magnetic interactions within two di-nuclear Dy^{III} complexes were elaborated through magnetic investigations as well as *ab initio* calculations.